ADAPTIVE KALMAN FILTERING FOR ATTITUDE ESTIMATION WITH LOW-COST SENSORS FOR A UNIVERSITY SATELLITE

Thiago Felippe Kurudez Cordeiro, thiago_kurudez@yahoo.com.br
Jacques Waldmann, jacques@ita.br
Instituto Tecnológico de Aeronáutica, Dept. Systems and Control, 12228-900 São José dos Campos, SP, (12)39475993

Abstract. *The innovation-based adaptive estimation (IAE) algorithm has been investigated for tuning an extended Kalman filter that estimates attitude and angular rate from vector measurements provided by low-cost Sun sensors and magnetometer on board a university satellite. The measurement noise covariance matrix* ***R*** *is considered to be known, but the process noise covariance matrix* ***Q*** *calls for proper tuning. Tuning has been carried out by trial and error in a near-equatorial orbit. Estimation error during eclipses precluded closed-loop control due to significant estimation error. Changes in project changed the orbit to a near-polar one. The investigation has comprised two conditions. One condition has made use of IAE to continuously adapt the process noise covariance matrix* ***Q****, whereas in the second condition a fixed, representative* ***Q*** *obtained from IAE-based tuning has been selected prior to applying the conventional Kalman filter. The adaptive filter yielded acceptable estimation performance without need for a priori knowledge and the IAE algorithm demonstrated its feasibility for straightforward tuning of* ***Q****. Furthermore, the investigation indicates that conventional filtering tuned with a fixed, representative* ***Q*** *matrix produced by IAE-based filtering can perform better than the original, trial-and-error tuning, with the additional gain of potentially allowing for proper closed-loop satellite pointing and attitude stabilization during eclipses due to reduced estimation error.*

Keywords*: adaptive Kalman filtering, low-cost satellite, magnetometer, process noise matrix tuning, attitude estimation*

1. INTRODUCTION

ITASAT is a low-cost university satellite project. The satellite has Sun sensors and magnetometers, but no rate-gyros. When eclipses occur, the Sun sensors can not provide any information.

An extended Kalman filter estimates seven state components, four from the attitude quaternion and three from angular rate. The measurement noise covariance matrix **R** is considered to be known, but the process noise covariance matrix **Q** calls for proper tuning (Santos, 2008). Tuning has been carried out by trial and error in Santos (2008) for a near-equatorial orbit. Changes in the project resulted in the orbit changing to a near-polar one, thus calling for additional tuning. A faster and more accurate tuning method is desired.

Insufficiently known a priori statistics reduce the precision and introduces biases on the estimated Kalman filter states and can even lead to practical divergence of the filter (Mohamed, 1999). Also, frequently changing environment affects the filter estimation accuracy (Mohamed, 1999). An adaptive filter formulation has weaker reliance on the a priori statistical information due to its learning process, and the frequent adaptation of the statistical filter information goes hand in hand with the idea of having a dynamic system in a dynamic environment (Mohamed, 1999).

In the satellite attitude control system design, the process noise matrix **Q** is not known. Furthermore, the occurrence of eclipses changes the estimation environment. These facts indicate that the use of an adaptive filter can be a good choice.

The innovation-based adaptive estimation (IAE) algorithm will be investigated for tuning the process noise matrix. The investigation has comprised two conditions. One condition has made use of IAE to continuously adapt the process noise covariance matrix **Q**, whereas in the second condition a fixed, representative **Q** obtained from IAE-based tuning has been selected prior to applying the conventional Kalman filter. Both conditions will be tested via software simulation.

2. ADAPTIVE KALMAN FILTER

The principle underlying the adaptive Kalman filter is to have the filter residuals consistent with the corresponding theoretical covariance (Mehra 1972). An estimate of the covariance of the residual is obtained by averaging from the previous residual sequence over a sample window with length *N* (Hide 2003), as shown in Eq. (1).

$$\hat{\mathbf{C}}_{v_k} = \frac{1}{N} \sum_{j=k-N+1}^{k} \mathbf{v}_j \mathbf{v}_j^T \tag{1}$$

N is a project parameter in the adaptive filter. Equation (1) is a maximum likelihood (ML) estimator and, as explained by Mohamed (1999), choosing a small sample window tends to make ML estimates biased. Enlarging the

window length makes the occurrence of bias less likely. However, as explained by Mohamed (1999), larger window lengths reduce the algorithm ability to correctly track high frequency changes in the environment. Therefore, the choice of *N* involves a trade-off between bias magnitude and agile tracking. Another point in the choice of *N* is that the adaptive filter can be turned on only after obtaining the first *N* data samples. Before that, the conventional filter must be used. However, for the intended application this is not a major point, because the simulation interval is very large, and the satellite sensors provide data at a relatively fast sample rate.

The innovation $\mathbf{v}_k$ is the difference between the measured value, $\mathbf{z}_k$, and the filter predicted value, $\mathbf{z}_k^-$, as shown in Eq. (2) and (3).

$$\mathbf{v}_k = \mathbf{z}_k - \mathbf{z}_k^- \tag{2}$$

$$\mathbf{z}_k^- = \mathbf{H}_k \hat{\mathbf{x}}_k^- \tag{3}$$

with $\mathbf{H}_k$ being the measurement matrix from the state-space model in the Kalman filter.

The estimated process noise matrix $\hat{\mathbf{Q}}_k$, known as residual-based estimate, can be obtained as in Eq. (4),:

$$\hat{\mathbf{Q}}_k = \frac{1}{N} \sum_{j=k-N+1}^{k} \Delta\hat{\mathbf{x}}_j \Delta\hat{\mathbf{x}}_j^T + \mathbf{P}_k^+ - \boldsymbol{\Phi}\mathbf{P}_{k-1}^+ \boldsymbol{\Phi}^T \tag{4}$$

with $\boldsymbol{\Phi}$ as the state transition matrix, $\mathbf{P}_k^+$ is the updated estimation error covariance computed by the Kalman filter, and $\boldsymbol{\Delta}\mathbf{x}$ is the state correction sequence, computed by Eq. (5).

$$\boldsymbol{\Delta}\mathbf{x}_k = \hat{\mathbf{x}}_k^+ - \hat{\mathbf{x}}_k^- \tag{5}$$

Using Eq. (6) and considering the filter in steady state, $\hat{\mathbf{Q}}_k$ can be approximated by Eq. (7) (Mohamed, 1999), known as innovation-based estimation:

$$\boldsymbol{\Delta}\mathbf{x}_k = \mathbf{K}_k \mathbf{v}_k \tag{6}$$

$$\hat{\mathbf{Q}}_k \approx \mathbf{K}_k \hat{\mathbf{C}}_{v_k} \mathbf{K}_k^T \tag{7}$$

with $\mathbf{K_k}$ is the Kalman filter gain. As in Hide (2003), it has been verified that changing all the non-diagonal terms to zero and maintaining the diagonal terms in $\hat{\mathbf{Q}}_k$ (in other words, ignoring cross correlations) provides better results than using the full matrix.

The measurement noise covariance $\hat{\mathbf{R}}_k$ can also be estimated, using Eq. (8). However, it will be assumed here that the measurement noise covariance is known as follows:

$$\hat{\mathbf{R}}_k = \hat{\mathbf{C}}_{v_k} - \mathbf{H}_k \mathbf{P}_k^- \mathbf{H}_k^T \tag{8}$$

Where $\mathbf{P}_k^-$ is the Kalman predicted estimation error covariance matrix.

3. SIMULATION SOFTWARE

The simulation software is based on the Simulink toolbox from Matlab. The simulation has included synthesizing magnetometer data, an extended Kalman filter to estimate magnetometer bias via preprocessing of raw magnetometer measurements (Alonso and Shuster, 2002a, 2002b), errors in the geomagnetic field model on board the satellite and in the orbit position estimation, and disturbance torques such as gravity gradient.

A near-polar orbit trajectory was simulated. The investigation focuses on estimation of open-loop dynamics, and thus actuators and control system were not simulated. Three conditions have been considered in satellite motion: tumbling, spinning and slow. Table 1 defines the motions profiles.

Those motion profiles are similar to the motion profiles used by Santos (2008). However, the initial attitude quaternion has been modified to simulate, in the near-polar orbit, the worst case scenario in tumbling and slow motion profile, and the correct satellite spin axis pointing in the case of the spinning motion profile. The worst case scenario is when the Sun is lighting sensitive areas from satellite and makes sense only when analyzing attitude control algorithms. This scenario has been chosen to maintain the previously used motion profiles and then test them in the near-polar orbit.

Table 1. Motion profiles.

Motion	Initial angular velocity ω_0 [rad/s]	Initial attitude quaternion q_0
Tumbling	$[8.73\cdot10^{-2}\ 8.73\cdot10^{-2}\ 8.73\cdot10^{-2}]^T$	$[0.5490\ 0.8306\ 0.0780\ 0.0515]^T$
Spinning	$[0\ 0\ 4.18]^T$	$[0.8879\ 0.1842\ -0.0856\ 0.4127]^T$
Slow	$[1.0\cdot10^{-6}\ 1.0\cdot10^{-6}\ 1.047\cdot10^{-3}]^T$	$[0.5490\ 0.8306\ 0.0780\ 0.0515]^T$

The satellite sensors and the Kalman filter run with a sample rate of 10 Hz. The sample window length N=30 has been defined, which results in a 3-second window length. Tighter windows have resulted in the system becoming unstable, while wider values impaired adaptation to on/off eclipses switches.

Two performance criteria have been used, namely Eqs. (9) and (10). They measure, respectively, the attitude and angular velocity estimation performance. Both are always positive and their values approach zero as the estimates approach the ground-truth values (Santos, 2008).

$$I_k = \left| \cos^{-1}\left(\tfrac{1}{2} trace\left(\mathbf{D}^T(\hat{\mathbf{q}}_{k|k}) \cdot \mathbf{D}(\mathbf{q}_k)\right) - \tfrac{1}{2}\right)\right| \tag{9}$$

$$F_k = \left[\left(\hat{\boldsymbol{\omega}}_{k|k} - \boldsymbol{\omega}_k\right)^T \cdot \left(\hat{\boldsymbol{\omega}}_{k|k} - \boldsymbol{\omega}_k\right)\right]^{\frac{1}{2}} \tag{10}$$

In Eq. (5), $\mathbf{D}(\mathbf{q}_k)$ is the DCM (Direct Cosine Matrix) derived from the actual quaternion $\mathbf{q}_k$. Likewise, $\mathbf{D}^T(\hat{\mathbf{q}}_{k|k})$ is the transpose of the DCM associated with the estimated quaternion $\hat{\mathbf{q}}_{k|k}$. In Eq. (6), $\boldsymbol{\omega}_k$ and $\hat{\boldsymbol{\omega}}_{k|k}$ are, respectively, the ground-truth and the estimated angular velocity.

The conventional and the adaptive filters have been simulated using 50 Monte Carlo trials each. Parameters of interest, like the performance criteria and the estimated process noise covariance, were stored. Then, the mean and variance of these parameters were computed.

4. RESULTS

Figure 1 shows eclipses during the near-polar orbit for all simulations. When eclipses occur, Sun sensors become inoperative. Tumbling and spinning motions have been simulated during 20 thousand seconds, whereas slow motion has been simulated for 40 thousand seconds. A far longer simulation time is needed to investigate and analyze the results arising from slow satellite motion, because the time needed by the estimators to converge were so much larger with respect to the other two motion profiles.

4.1. Conventional versus adaptive filter

Firstly, the conventional filter has been simulated with the $\mathbf{Q}$ matrix tuned by trial and error in Santos (2008). This tuning has used the same sensors though in a distinct orbit. The approach has yielded adequate performance in the low-inclination, near-equatorial orbit (Santos, 2008), but diverged in the near-polar orbit. The estimator presented severely degraded estimation errors during eclipses.

Then, the adaptive (IAE) filter was simulated. The results were far better as the estimation error grew quite slowly during eclipses. In the first eclipse, the estimation performance was lacking because both the magnetometer bias estimator and the process noise covariance estimator had not fully converged yet. Figure 2 compares the attitude and angular velocity estimation performance of both the conventional and the adaptive filters. The comparison shows the mean value of the performance criteria I_k and F_k plus three times the standard deviation derived from 50 Monte Carlo trials.

Figure 3 shows two graphics. To the left is shown the time evolution of the diagonal element in the estimated process noise covariance related to the real component λ of the attitude quaternion. This estimate is the tuned variance in the λ component, which has been computed with the IAE algorithm as the satellite undergoes the tumbling motion. The remaining diagonal elements are related to the tuned variances of the imaginary components of the attitude quaternion and present similar results. Thus, they have been omitted from the plot. To the right are displayed the

estimated variances corresponding to the diagonal elements that are related to the angular rate components. The values from both graphics have been computed from the average mean of 50 Monte Carlo trials.

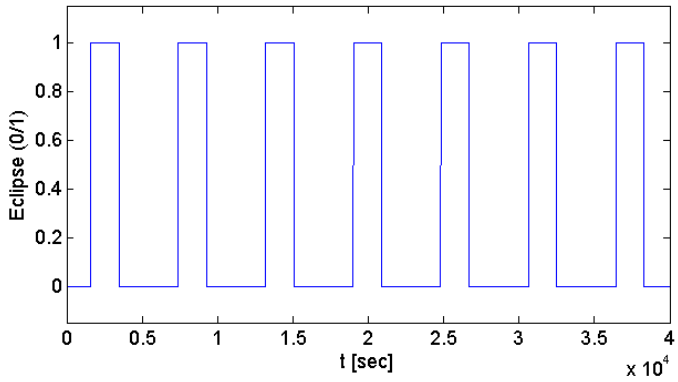

Figure 1. Occurrence of eclipses. The value "one" indicates an eclipse.

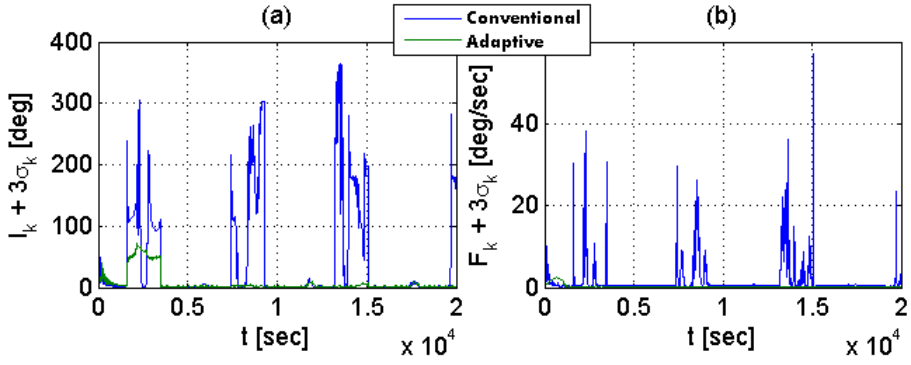

Figure 2. Attitude (a) and angular velocity (b) estimation performance in the tumbling motion. Conventional versus adaptive Kalman filter. The adaptive filter is barely visible in both cases due to its superior performance.

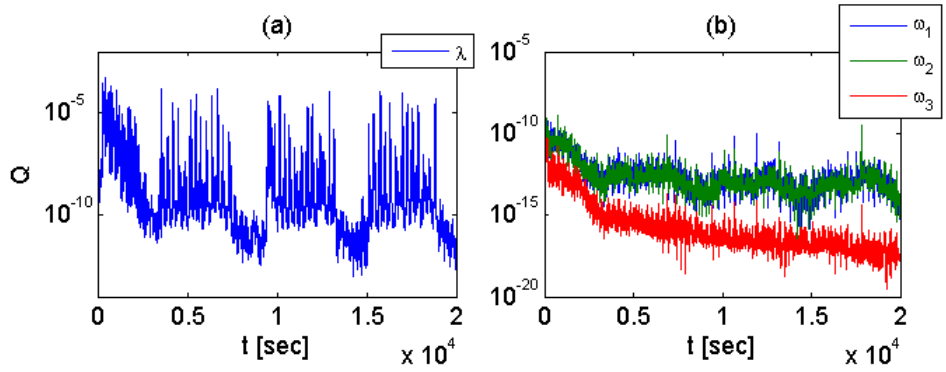

Figure 3. Estimated process noise variance during tumbling motion corresponding to the real component λ of the attitude quaternion (a), and the variances corresponding to the angular velocity components (b). Notice the semi-log scale.

Inspecting the diagonal term of the adapted **Q** related to the real component λ in Fig. 3, after the first 4 thousand seconds (after convergence of both bias and attitude estimators), it can be seen that the process noise covariance estimation is different depending on the occurrence of eclipses. A quite smaller average value has been noticed during eclipses in comparison with the average value out of the eclipses. Therefore, knowing that the **Q** matrix is a parameter that indicates to the Kalman filter the level of uncertainty in the dynamics model, the IAE algorithm provided,

respectively, more confidence in the model during eclipses, and more confidence in the measurements when both Sun sensor and magnetometer were functional. This fact shows that the filter can adapt to environmental changes.

Inspecting the diagonal term of the adapted **Q** related to the angular velocity components in Fig. 3 it can be seen that this estimation oscillates around a quite stable value, and has remained unaffected regardless of the occurrence of eclipses.

4.2. Adjusting the conventional filter based on adaptive filtering results

The conventional filter has been tuned using fixed diagonal entries arising from the geometric time average of the adapted **Q** matrix. Equation (11) shows how the geometric time average has been computed, where k_0 and k_f define the initial and the final time instants of the averaging time window, $\hat{\mathbf{Q}}$ is the tuned **Q** matrix, and recall that $\hat{\mathbf{Q}}_j$ is diagonal.

$$\hat{\mathbf{Q}} = \exp\left(\frac{1}{k_f - k_0} \sum_{j=k_0}^{k_f} \ln \hat{\mathbf{Q}}_j \right) \tag{11}$$

The geometric time average has been proposed intuitively based on the fact that the estimated process noise covariance plots in Fig. 3 are more meaningful with a vertical semi-log scale. Both geometric and arithmetic time average have been tested to generate a tuned **Q** matrix, and the geometric average yielded much better results.

Table 2. Original and adjusted tuning of the diagonal elements of the process noise covariance **Q**.

Diagonal element	Previous tuning	Geometric time average tuning	Geometric time average tuning – adjusted
λ	$8.0 \cdot 10^{-6}$	$4.9737 \cdot 10^{-10}$	$4.9737 \cdot 10^{-10}$
q_1	$8.0 \cdot 10^{-6}$	$4.8655 \cdot 10^{-10}$	$4.8655 \cdot 10^{-10}$
q_2	$8.0 \cdot 10^{-6}$	$5.1972 \cdot 10^{-10}$	$5.1972 \cdot 10^{-10}$
q_3	$8.0 \cdot 10^{-6}$	$4.2825 \cdot 10^{-10}$	$4.2825 \cdot 10^{-10}$
ω_1	$2.0 \cdot 10^{-5}$	$1.7680 \cdot 10^{-13}$	$1.7680 \cdot 10^{-13}$
ω_2	$2.0 \cdot 10^{-5}$	$1.5885 \cdot 10^{-13}$	$1.5885 \cdot 10^{-13}$
ω_3	$2.0 \cdot 10^{-5}$	$1.3119 \cdot 10^{-16}$	$1.6783 \cdot 10^{-13}$

The adapted **Q** matrix was obtained from simulation with the tumbling motion. Distinct motion profiles have called for different tuning results, but the tuning obtained when the satellite was subject to tumbling motion has provided so far the most significant improvement in estimation performance.

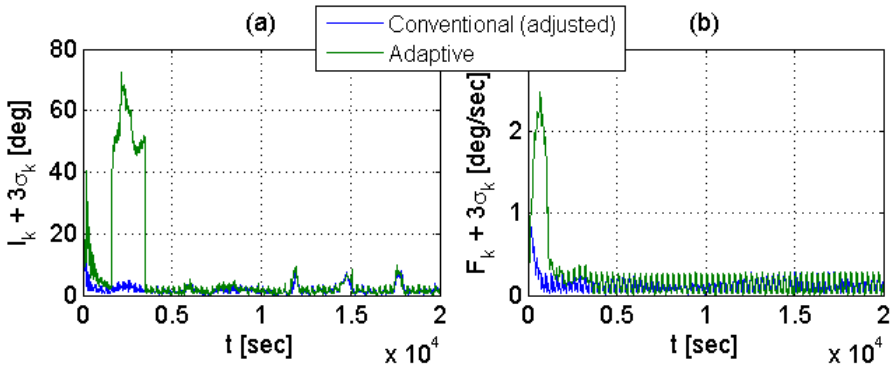

Figure 4. Attitude (a) and angular velocity (b) estimation performance under tumbling motion. Adjusted conventional Kalman filter versus adaptive Kalman filter.

However, when undergoing the spinning motion with the above tuned **Q**, the estimate of the angular rate component along the spinning axis, ω_3, was quite degraded, which caused the attitude estimation to slowly diverge. Then, the corresponding ω_3 process noise variance has been empirically adjusted to a value closer to the estimated variances of ω_1 and ω_2. This adjustment made the filter to stop diverging when the satellite was subject to the spinning motion, and resulted in a slight improvement for the remaining motion profiles. Table 2 shows the obtained tuning results.

Figures 4, 5 and 6 show the estimation performance when the satellite has been subjected to, respectively, tumbling, spinning and slow motion, for both the adaptive and the tuned conventional filter.

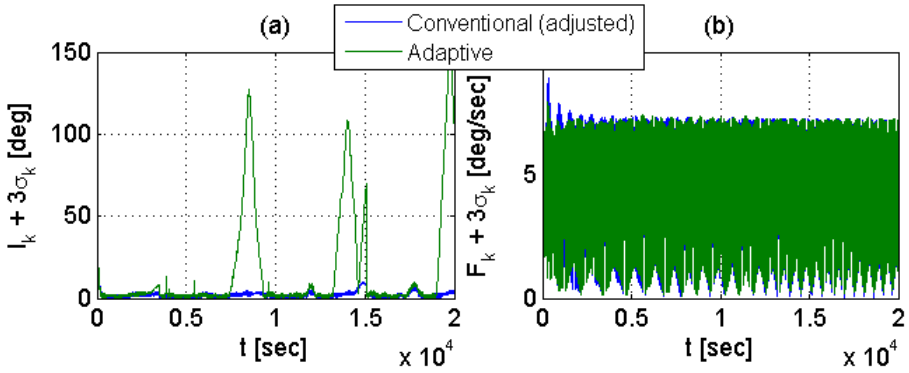

Figure 5. Attitude (a) and angular velocity (b) estimation performance under spinning motion. Adjusted conventional Kalman filter versus adaptive Kalman filter.

In Figure 4, it is possible to see that the results from both filters are very similar. In the first eclipse, the adaptive filter yielded degraded performance because it has not converged yet.

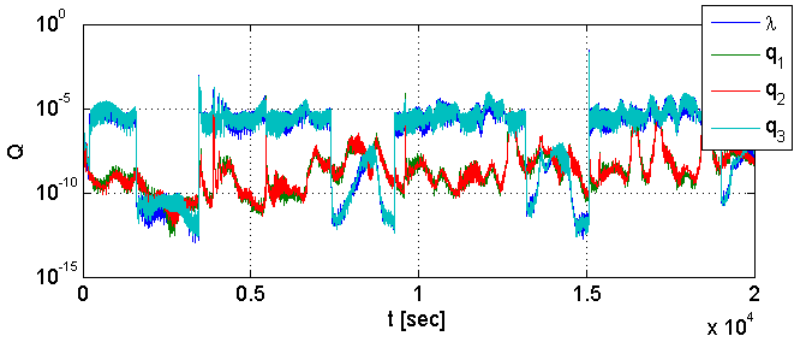

Figure 6. Estimated process noise variances corresponding to attitude quaternion components during spinning motion. Notice the semi-log scale.

In Figure 5, both filters work well when there is no eclipse. In both filters, however, the angular rate estimation is relatively poor because the spinning axis rotates at 40 RPM, which is relatively fast for the 10 Hz sensor sampling frequency. In this case of spinning, the conventional filter performs much better than the adaptive one when the satellite undergoes eclipses.

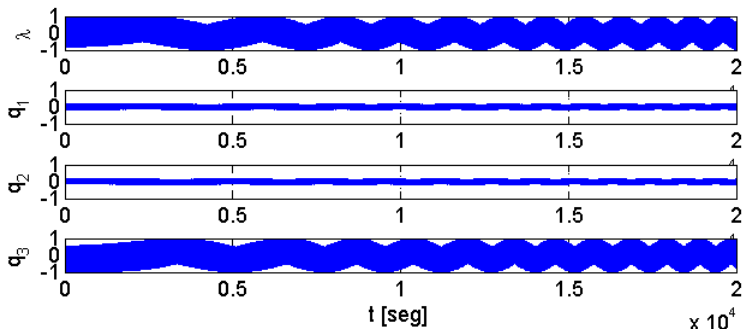

Figure 7. Ground-truth attitude quaternion during spinning motion.

The initial five thousand seconds in Fig. 5 show that the first eclipse does not yield performance degradation of the adaptive filter as much as is caused by the following eclipses. Looking at Fig. 6, the estimated covariances of components q_1 and q_2 have magnitudes close to 10^{-10} near the start of the first eclipse, which agrees with the magnitudes

obtained during tumbling motion (Fig. 3) and the magnitudes obtained by the geometric average (Table 2). In the following eclipses, the magnitudes of the estimated covariance of components q_1 and q_2 are not as close to 10^{-10} as in the first eclipse. This incorrect covariance estimation might give rise to a slow divergence in attitude estimation, but further investigation into such a matter is in order.

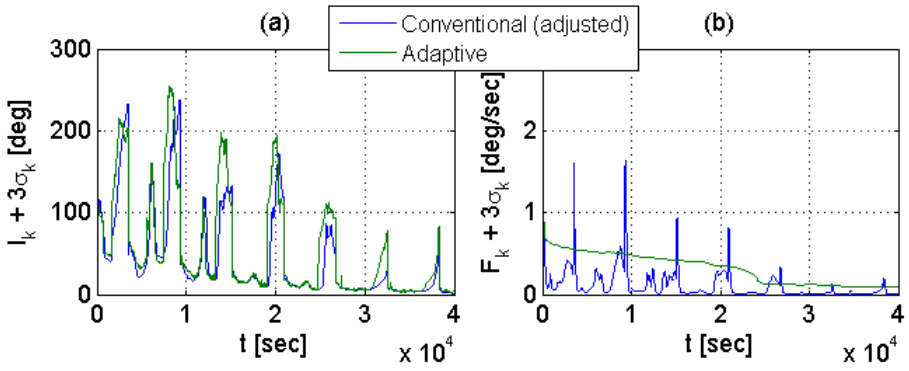

Figure 8. Attitude (a) and angular velocity (b) estimation performance under slow motion. Adjusted conventional Kalman filter versus adaptive Kalman filter.

Figure 7 shows the ground-truth attitude quaternion for the spinning motion profile. Looking at the quaternion components q_1 and q_2, it is possible to see that they vary much less than the other components. This observation may explain why the estimation of the covariance of these quaternion components is degraded, as spinning motion does not provide an adequate excitation signal to these particular quaternion components. This may also explain why tumbling motion provides improved tuning using the geometric average: such motion provides a better excitation signal.

In Figure 8, the attitude and angular rate estimations are much degraded during the first 20 thousand seconds. This is due the converging time of the bias estimator being significantly larger when the satellite undergoes slow motion than in the former motion profiles. Comparing both filters, the adjusted conventional filter, again, shows better results most of the time.

5. CONCLUSION

Adaptive filtering is an attractive option in highly uncertain environments, and yields acceptable estimation performance without need for a priori knowledge. For example, in case the design of the attitude control system should be modified for satellite operation with different orbit parameters due to changing launch vehicle constraints, trial-and-error, adaptive filtering can be an attractive alternative to manual, trial-and-error tuning of the filter.

Furthermore, the conventional filter with adjusted process noise covariance does yield improved performance with respect to the straightforward use of the innovation-based adaptive filter. The adjustment has been accomplished by means of an investigation of the adaptive filter performance. Also, considering that the computational resources on board the satellite are limited, and that the workload of the conventional filter is much lighter than that of the adaptive filter, the former with the adjusted process noise covariance becomes a better choice for the satellite.

The adaptive filter, although not the most viable option for real-time implementation in the satellite, has become a quite useful tool for off-line filter tuning. With a few simulations and a geometric time average of the results, it has been possible to compute an adequate estimate of the process noise covariance **Q** matrix.

Therefore, the investigation indicates that conventional filtering tuned with a fixed, representative **Q** matrix produced by innovation-based adaptive filtering yields superior performance relative to the original, trial-and-error tuning in Santos (2008), with the additional gain of potentially allowing for proper closed-loop satellite pointing and attitude stabilization during eclipses due to remarkably reduced estimation errors.

6. ACKNOWLEDGEMENTS

The authors acknowledge the support provided by project FINEP/CTA/INPE SIA (Sistemas Inerciais para Aplicação Aeroespacial).

7. REFERENCES

Alonso, R; Shuster, M.D., 2002a. “TWOSTEP: A Fast Robust Algorithm for Attitude-Independent Magnetometer Bias Determination”. The Journal of the Astronautical Sciences, Vol. 50, No. 4, pp. 433-451.

Alonso, R; Shuster, M.D., 2002b. "Complete Linear Attitude-Independent Magnetometer Calibration". The Journal of the Astronautical Sciences, Vol. 50, No. 4, pp. 477-490.

Hide, C., Moore, T. and Smith, M., 2003. "Adaptive Kalman Filtering for Low-cost INS/GPS". Journal of Navigation, Vol. 56, No. 1, pp. 143-152.

Mehra, R.K., 1972. "Approaches to adaptive filtering". IEEE transactions on automatic control, Vol. 17, No. 5, pp. 693-698.

Mohamed, A.H. and Schwarz, K.P., 1999. "Adaptive Kalman filtering for INS/GPS". Journal of Geodesy, Vol. 73, No. 4, pp. 193-203.

Santos, D.A., 2008. "Estimação de Atitude e Velocidade Angular de Satélites Utilizando Medidas de Campo Geomagnético e Direção do Sol", M.Sc. thesis, Instituto Tecnológico de Aeronáutica, São José dos Campos, S. Paulo, Brazil, 157 p.

8. RESPONSIBILITY NOTICE

The authors are the only responsible for the printed material included in this paper.